IEEE Access
Multidisciplinary ⋮ Rapid Review ⋮ Open Access Journal

Received 25 October 2023, accepted 17 November 2023, date of publication 20 November 2023,
date of current version 29 November 2023.

Digital Object Identifier 10.1109/ACCESS.2023.3335329

RESEARCH ARTICLE

A Frequency Selective Absorber With Anisotropic Reflection Band for Radar Cross Section Reduction

ASAL MALEKARA, CHANGIZ GHOBADI, AND JAVAD NOURINIA, (Senior Member, IEEE)
Department of Electrical Engineering, Urmia University, Urmia 57561-51818, Iran
Corresponding author: Changiz Ghobadi (ch.ghobadi@urmia.ac.ir)

ABSTRACT In this paper, a frequency selective absorber (FSA) with an anisotropic reflection band is proposed for radar cross section (RCS) reduction applications. The presented design is a 2-D triple-layered structure consisting of a lossy frequency selective surface (FSS) at the top, a lossless FSS at the intermediate, and a metal plane at the bottom. All the layers of the proposed structure are printed on the low-cost FR4 substrate and separated by air spacers. The lossy FSS layer loaded with lumped resistors leads to a wide absorption band. The reflection band with anisotropic property is attained using the intermediate lossless FSS layer, constituted of two intersecting non-perpendicular dipole-shaped patches in each unit cell of the structure. By adjusting the angle between two dipole-shaped patches (2α), the location of the reflection bands can be tuned across the absorption band. Under the normal incidence, the presented design covers a wide absorption frequency range of 2.4 GHz to 8.3 GHz, where the reflection coefficient is below -10 dB (fractional bandwidth $= 110\%$). Considering $\alpha = 35°$, the reflective notch frequencies at $f_{TE} = 4.47$ GHz and $f_{TM} = 5.74$ GHz are attained under transverse-electric (TE) and transverse-magnetic (TM) polarizations, respectively. To validate the performance of the proposed design, a prototype was fabricated and measured. The results demonstrate good agreement between the measured and simulated data.

INDEX TERMS Frequency selective surface, frequency selective absorber, radar cross section, anisotropic reflection band, equivalent circuit model.

I. INTRODUCTION

Over the past years, absorbers have found a wide variety of applications, such as interference reduction and radar cross-section (RCS) reduction [1], [2], [3], [4]. Unlike traditional absorbers, frequency selective absorbers (FSA) have either a transmission band (FSA-T) or a reflection band (FSA-R) [5], [6], [7], [8]. The FSA-T are the structures placed in front of the antennas as radomes, allowing electromagnetic (EM) waves of a certain frequency to transmit with low insertion loss while absorbing the out-of-passband waves [9], [10], [11], [12], [13]. On the contrary, FSA-R reflects EM waves at a specific frequency instead of transmission and absorbs the incoming waves in the other range [14], [15], [16]. The most common usage of this type of FSA is exploiting it as the functional ground of the antennas [17]. In this case, the FSA-R is designed such that its reflection band coincides with the operating band of the antenna to maintain or enhance the antenna's gain and absorbs out-of-band impinging waves upon the antenna for substantial backscattering reduction [18], [19], [20], [21], [22], [23].

FSA-Rs can be constructed in 2-D or 3-D forms. In [19], Sharma et al. introduced a polarization-independent 2-D triple-layered FSA-R with a flat reflection band between two absorption bands. In [20], Han et al. designed a dual-polarized, two-layered planar FSA with a notched band within a broad absorption frequency range. In [24], a 3-D FSA-R was reported, demonstrating a flat reflection band and two wide absorption bands on both sides. Although 3-D structures offer advantages, such as achieving higher-order filtering responses, they come with increased fabrication complexity and higher costs. On the contrary,

The associate editor coordinating the review of this manuscript and approving it for publication was Chinmoy Saha.

the 2-D structures feature simple and flexible designs, making them suitable and preferable for various applications [19], [25]. Besides, all of the aforementioned studies on FSA-R have a symmetric shape and offer the same electromagnetic responses to orthogonal transverse-electric (TE) and transverse-magnetic (TM) polarized waves. However, many realistic applications require distinct frequency characteristics for different polarizations to improve detection and anti-interference performance [26], [27], [28]. For instance, these structures are well-suited for military applications where directionality, beamforming, and signal control are essential for secure and reliable communication [29]. Anisotropic structures can be attained by incorporating asymmetrical elements in the design of unit cells within the periodic structures.

To the author's best knowledge, previous papers have not demonstrated FSA-R with an anisotropic reflection band. Therefore, this paper focuses on the design and structure implementation of a 2-D FSA-R with an anisotropic reflection band. The top layer of the proposed structure is a lossy FSS whose contribution is producing a wide absorption band. Owing to the symmetry of this layer, the absorption band for both TE and TM polarizations is the same. The bottom layer is a copper-cladded sheet that acts as the ground plane. A lossless FSS is embedded as the intermediate layer of the structure to introduce a notch in the absorption band. In order to have distinct notch frequencies for different polarizations and make the reflection band anisotropic, two intersecting non-perpendicular dipole-shaped patches are considered as the unit cell of the intermediate layer. The frequencies of the reflection band can be adjusted by varying the angle between the dipole patches (2α). Both the FSS layers of the presented structure are printed on the low-cost FR4 ($\varepsilon_r = 4.4$, tan $\delta = 0.02$) substrate. All the metallic parts of the proposed FSA-R are made of 0.035 mm thick copper, with a conductivity of 5.8×10^7 S/m. Under the normal incidence, the presented design covers a wide absorption frequency range of 2.4 GHz to 8.3 GHz, where the reflection coefficient is below -10 dB (fractional bandwidth = 110%). By considering $\alpha = 35°$, the reflective notch frequencies of $f_{TE} = 4.47$ GHz and $f_{TM} = 5.74$ GHz are attained under TE and TM polarizations, respectively. The results prove that the proposed FSA-R is a suitable candidate to serve as the ground plane of the antennas operating in distinct frequencies for orthogonal polarizations, aiming to reduce RCS. The complete specifications and design procedure are provided in great detail in the following sections. Also, an equivalent circuit model (ECM) accompanies the presented descriptions to provide a deeper physical insight into the proposed structure.

The rest of the paper is organized as follows: Section II argues about the theoretical analysis of the proposed structure. The design methodology of the proposed FSA-R is explained, and some simulations were carried out to evaluate the performance of the presented structure in Section III. In Section IV, additional simulations are performed to further assess the design's validity. A prototype of the proposed FSA-R was fabricated and measured, and a performance comparison with previous works is given in Section V. Finally, concluding remarks are provided in Section VI.

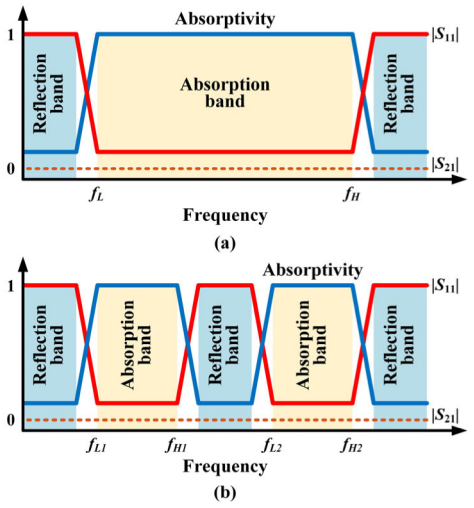

FIGURE 1. Frequency response of (a) a typical absorber and (b) an FSA-R.

II. THEORETICAL ANALYSIS

Fig. 1(a) illustrates the frequency response of a typical absorber. In the working band, both reflection and transmission coefficients are small, meaning that this structure absorbs all incident waves. However, the mentioned characteristic does not meet all requirements in several RCS reduction applications. In these cases, there is a need to provide a bandstop filtering response within the absorption band. This kind of FSA structure is known as FSA-R. The general frequency response of an FSA-R structure is illustrated in Fig. 1(b). A strong reflection is inserted in the middle of the absorption band [23]. Theoretical analysis and design procedure of the FSA-R are provided in the following sections.

A. THEORETICAL ANALYSIS OF ABSORBER

The first step of designing the proposed FSA-R is constructing a wideband absorber.

As represented in Fig. 2(a), a typical dual-layered absorber comprises a lossy FSS layer and a metal plane separated by a dielectric spacer with the thickness of t [30], [31]. With regard to the transmission line theory [32], the general ECM of this structure can be considered, as shown in Fig. 2(b). The shunt impedance of Z_R denotes the equivalent impedance of the lossy FSS layer. Due to the lossy property of the top layer, Z_R is a complex impedance and is expressed as $Z_R = R_R + jX_R$. Assuming the bottom layer is a perfect metal plane, its impedance is considered near zero (short circuit). $Z_0 = 120\pi$ and $Z_S = Z_0/\sqrt{\varepsilon_r}$ are the characteristic impedance of the free space and the dielectric spacer, respectively.

An ideal absorber should fully absorb incoming waves without any power being transmitted or reflected. In other words, both $|S_{11}|$ and $|S_{21}|$ should equal zero, well-known as the perfect absorption condition [33]. $|S_{21}| = 0$ is satisfied due

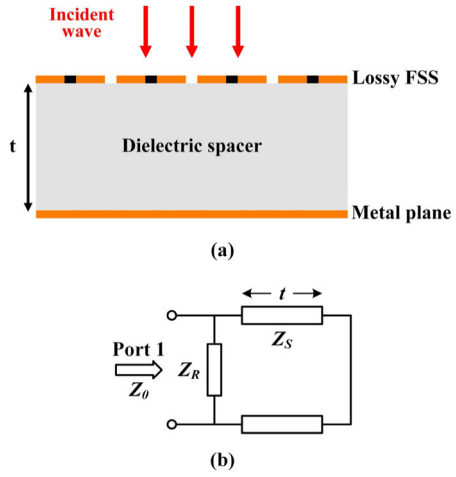

FIGURE 2. (a) Structure and (b) ECM of a typical dual-layered absorber.

to the presence of a metal plane on the back of the absorber structure. To fulfill the criteria of $|S_{11}| = 0$, the reflection coefficient formula has to be investigated.

$$|S_{11}| = \left| \frac{-(R_R \cos\delta + X_R \sin\delta) + j\left[(R_R - Z_0)\sin\delta - X_R \cos\delta\right]}{(R_R \cos\delta - X_R \sin\delta) + j\left[(R_R + Z_0)\sin\delta + X_R \cos\delta\right]} \right| \tag{1}$$

where $\delta = \beta t = {}^{2\pi t}/_{\lambda} = {}^{2\pi tf}/_{c}$ is the equivalent phase path of the dielectric spacer. According to equation (1), R_R and X_R should be in the following form to meet the perfect absorption condition ($|S_{11}| = 0$):

$$R_R = Z_0 \sin^2\delta \tag{2}$$

$$X_R = -Z_0 \sin\delta \cos\delta \tag{3}$$

In practice, designing a perfect absorber with a fixed value of δ over a wideband frequency range is very difficult. Instead of perfect absorptivity, a general absorption condition (GAC) is considered for real and imaginary parts of the lossy layer impedance in which $|S_{11}| < -10$ dB (Fig. 3) [34].

B. THEORETICAL ANALYSIS OF THE FSA-R

As illustrated in Fig. 4(a), one can form an FSA-R structure by inserting a lossless FSS between the lossy FSS and the metal plane of an absorber. Indeed, adding the lossless FSS layer introduces a notch in the absorption band, as shown in Fig. 1(b) [19].

The theoretical analysis, which is performed in the following, indicates that notch frequency is solely determined by the specifications of the lossless FSS layer. The ECM of a typical FSA-R structure is provided in Fig. 4(b). In this equivalent circuit, the lossless FSS is modeled as a shunt impedance of Z_B, which is purely imaginary ($Z_B = jX_B$). Z_{S1} and Z_{S2} are the characteristic impedances of the upper and lower dielectric spacers, respectively. The ABCD matrix of the ECM of Fig. 4(b) is a product of two cascaded matrixes

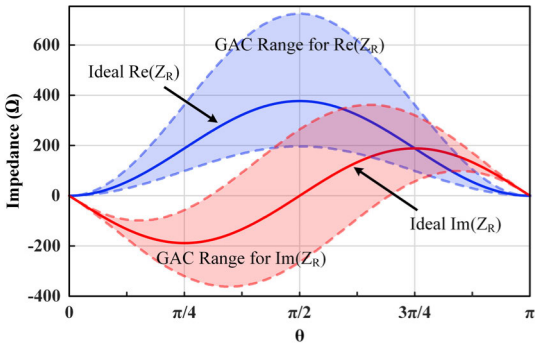

FIGURE 3. Impedance range of Z_R according to the GAC condition.

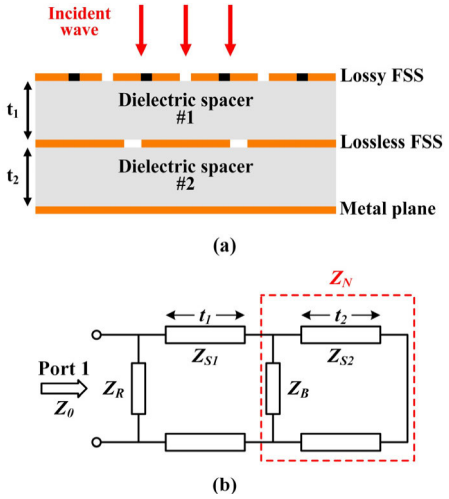

FIGURE 4. (a) Structure and (b) ECM of an FSA-R.

as follows [22]:

$$\begin{bmatrix} A & B \\ C & D \end{bmatrix} = \begin{bmatrix} 1 & 0 \\ \dfrac{1}{Z_R} & 1 \end{bmatrix} \begin{bmatrix} \cos\delta_1 & jZ_{S1}\sin\delta_1 \\ j\dfrac{\sin\delta_1}{Z_{S1}} & \cos\delta_1 \end{bmatrix} \tag{4}$$

where $\delta_1 = \beta t_1 = (2\pi t_1/c)f$ is the total phase path of the upper dielectric spacer. Based on the relationship between the transformation ABCD matrix and the S-parameter matrix, the reflection coefficient (S_{11}) can be expressed in the form of equation (5) [32]. The lossless FSS, the lower dielectric spacer, and the metal plane, which are marked with a red dotted box, together can be treated as a reactive load of $Z_N = jX_N$ for the sake of simplicity.

$$|S_{11}| = \left| \frac{AZ_N + B - CZ_0Z_N - DZ_0}{AZ_N + B + CZ_0Z_N + DZ_0} \right| \tag{5}$$

An ideal FSA-R structure should reflect all the incident waves at the reflective notched band. In other words, $|S_{11}|$ should be equal to 1. By doing so, Z_N would be in the following form:

$$Z_N = jX_N = -jZ_0 \tan\delta_1 \tag{6}$$

Hence, the notch frequency f_N is:

$$f_N = \frac{c}{2\pi t_1} \arctan\left(-\frac{X_N}{Z_0}\right) \tag{7}$$

As is clear, the lossy layer (Z_R) impedance has no effect on the notch frequency. Supposing the thickness of the upper dielectric spacer would be fixed, the notch frequency only depends on the value of the reactance X_N. Thus, the structure of the lossless FSS layer determines the reflection frequency.

III. DESIGN OF THE STRUCTURE

Fig. 5(a) and (b) illustrate the frequency response of a typical FSA-R with an anisotropic reflection band under TE and TM polarization incident waves, respectively. As seen, the absorption bands of both polarizations are the same, while the position of the notch frequencies is different.

The design procedure to realize an FSA-R with an anisotropic reflection band is as follows. The initial step is the design of a wideband absorber consisting of a lossy FSS layer at the top and a metal plane at the bottom. Next, a lossless FSS layer is inserted between two layers to incorporate a reflection band within the absorption band of the absorber. To realize an FSA-R with an anisotropic reflection band, an asymmetrical design should be considered for the mentioned lossless FSS layer, which leads to different notch frequencies under the TE and TM polarizations.

A. DESIGN OF ABSORBER

The unit cell of the designed wideband absorber is shown in Fig. 6. It consists of a lossy FSS, a supporting FR4 substrate, an air spacer, and a metal plane. The FR4 substrate has a relative permittivity of $\varepsilon_r = 4.4$ and a loss tangent of tan $\delta = 0.02$. The lossy FSS comprises a Jerusalem cross element with a resistor-loaded ring loop at the center. Fig. 7(a) shows the acceptable GAC range of the impedance of the lossy FSS ($Z_R = R_R + jX_R$). The values of R_R and X_R of the freestanding lossy FSS are obtained using full-wave simulation software CST Microwave Studio. CST uses the Floquet analysis to predict the response of the periodic structures.

This approach reduces the calculations of the complete structure into a single unit cell and assumes infinite repetition of unit cells on its four sides to realize periodic boundary conditions. The exciting wave is defined by Floquet port as a normally incident plane wave with an electric field polarized along the y and x axis for TE and TM polarized waves, respectively [35]. As shown in Fig. 7(a), both R_R and X_R are well within the GAC range at 2.35 - 8.30 GHz. Fig. 7(b) illustrates the reflection coefficient of the whole absorber obtained from the CST. The band of $|S_{11}| < -10$ dB covers 2.40 to 8.30 GHz.

B. DESIGN OF FSA-R

As stated in Section II, the next step for realizing an FSA-R is inserting a lossless FSS layer between two layers of the absorber to introduce a notch in the absorption band. Fig. 8 shows the complete unit cell of the proposed FSA-R. The geometry of this structure was determined by the built-in optimization techniques of CST software to meet design requirements. As seen, the lossless FSS of this structure is composed of two dipole-shaped patches, which are supported

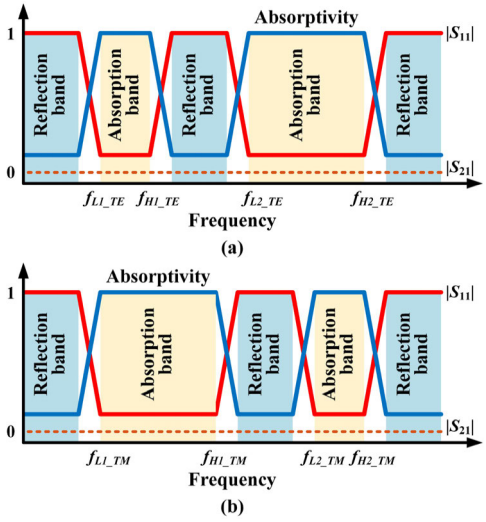

FIGURE 5. Frequency response of a typical FSA-R with an anisotropic reflection band under (a) TE and (b) TM polarization incident waves.

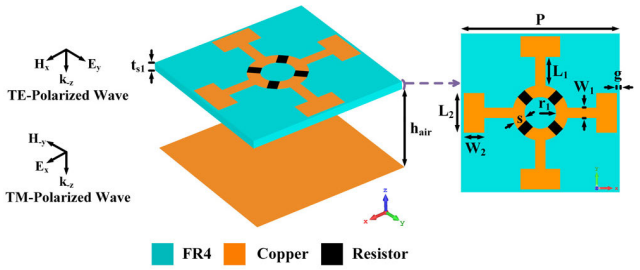

FIGURE 6. The unit cell of the proposed wideband absorber. Dimension in millimeter: P = 20, g = 0.25, W_1 = 1.1, W_2 = 3.6, L_1 = 2.5, L_2 = 5, r_1 = 2.1, s = 1.6, h_{air} = 11.5, t_{s1} = 1.

by an FR4 substrate with 0.5 mm thickness. The deformation at the end of patches increases terminal capacitance, and hence, notch resonance shifts to a lower frequency despite the constant dimensions. In other words, a compact structure with higher angular stability has been achieved in this way. To make the reflection band anisotropic, the mentioned diploes are considered non-perpendicular to each other. By varying the angle between two dipole-shaped patches (2α), the interaction of the structure with incoming electromagnetic waves alters in TE and TM polarizations. Thus, different anisotropic responses can be accomplished. Fig. 9 illustrates the reflection coefficient of the proposed FSA-R in the case of a simple cross-dipole patch and an end-deformed cross-dipole patch as the intermediate layer.

Fig. 10(a) shows the co-polarized reflection coefficient and absorptivity of the proposed FSA-R under normal incidence. Due to the presence of a metal plane on the back of the structure, the absorptivity can be calculated by $1 - |S_{11}|^2$. These results prove that an FSA-R with an anisotropic reflection band is achieved.

By considering $\alpha = 35°$, the reflective notch frequencies are $f_{TE} = 4.47$ GHz and $f_{TM} = 5.74$ GHz with 0.8 dB and 0.9 dB reflection loss under TE and TM polarizations, respectively. Despite using FR4 substrates, the presented work has

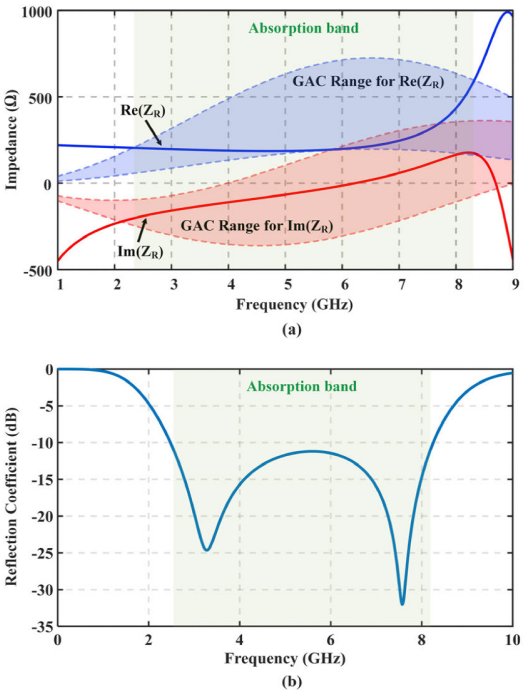

FIGURE 7. Simulation results of the proposed absorber. (a) Impedance and (b) Reflection Coefficient.

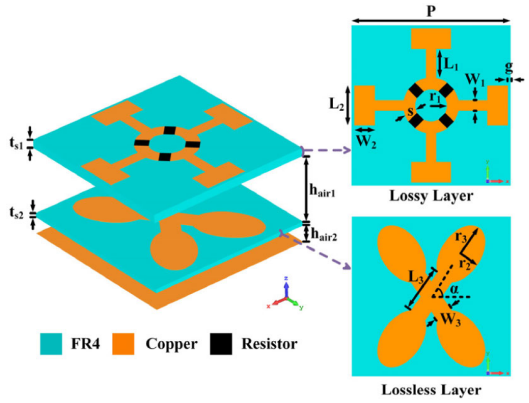

FIGURE 8. The unit cell of the proposed FSA-R. Dimension in millimeter: $P = 20$, $g = 0.25$, $W_1 = 1.1$, $W_2 = 3.6$, $W_3 = 2.2$, $L_1 = 2.5$, $L_2 = 5$, $L_3 = 5.8$, $r_1 = 2.1$, $r_2 = 2.5$, $r_3 = 4$, $s = 1.6$, $h_{air1} = 8$, $h_{air2} = 2$, $t_{s1} = 1$, $t_{s2} = 0.5$.

a reasonable loss. To examine the impact of the dielectric, the simulation was performed again by considering the loss factor of FR4 equal to the loss factor of Rogers 4350B (tan $\delta = 0.0037$). By doing so, the amount of loss becomes 0.2 dB for both TE and TM polarized waves, indicating a slight reduction compared to the previous design specification. The cross-polarized reflection coefficient simulation result is provided in Fig. 10(b) to investigate the polarization independence of the overall structure. As seen, S_{11} is always lower than -60 dB, indicating that the presented FSA-R has excellent polarization isolation.

Fig. 11 illustrates the effect of the variation of α angle on the overall performance of the proposed FSA-R. Based on the obtained results, notch frequencies alter by changing the angle between two dipole-shaped patches.

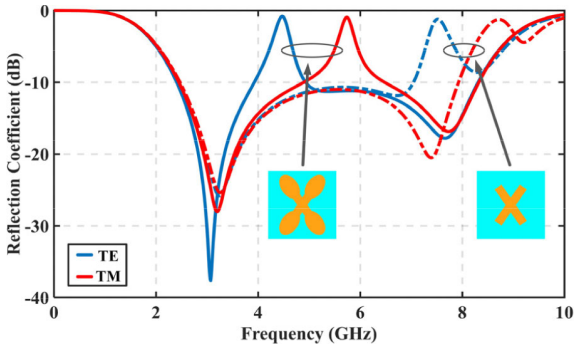

FIGURE 9. Design procedure of the intermediate layer of the proposed FSA-R.

IV. ECM AND ANALYSIS OF THE PROPOSED FSA-R

A. EQUIVALENT CIRCUIT MODEL

Fig. 12 illustrates the ECM of the proposed FSA-R under a normal incident wave. The free space and substrates are modeled as transmission lines of corresponding electrical length with characteristics impedance of $Z_0 = 377\ \Omega$ and $Z_{Sub} = 377/\sqrt{\varepsilon_r} = 179.7\,\Omega$, respectively. The lossy FSS is equivalent to a series RLC, and the lossless is represented by a series LC circuit. The capacitance C_3 is introduced to represent the coupling effect between the intermediate layer and the metal plane. The analytical equations have been used to obtain the values of the ECM parameters [36], [37].

Although there is a complex interaction between the different elements, some negligible components are not taken into account in the ECM for the sake of simplicity. The obtained values are considered as initial points of the optimization process in the Advanced Designed System (ADS) to improve the alignment of the full-wave simulation and ECM results. By doing so, the optimized values of the equivalent circuit components are: $R = 244\ \Omega$, $L_1 = 8.11$ nH, $C_1 = 155$ fF, $L_{2-TE} = 6.19$ nH, $C_{2-TE} = 135$ fF, $C_{3-\mathrm{TE}} = 94.78$ fF, $L_{2-TM} = 12.01$ nH, $C_{2-TM} = 49.44$ fF, $C_{3-TM} = 69$ fF. TE and TM indices distinguish the equivalent values of the different polarizations. The slight deviations in the resistance values between the ECM and CST simulations can be attributed to the use of first-order approximation (lumped) components in the ECM and variations in resistance with frequency, primarily due to the skin effect [38].

Fig. 13 compares the reflection coefficient obtained from CST and ECM. As is obvious, a good agreement exists between the results. A few discrepancies between the results can be attributed to the fact that CST software exploits a more complex and realistic model versus ECM. As stated before, ECM uses simple lumped elements, and its main objective is gaining a quick and straightforward insight into EM structure.

B. SURFACE CURRENT DISTRIBUTION

To gain an intuitive insight into the operating principle of the proposed FSA-R, the current distributions of the lossless FSS are investigated using the CST software at two reflection frequencies (4.47 and 5.74 GHz). Fig. 14 (a)-(b) shows the current distribution for TE polarized wave. In this case,

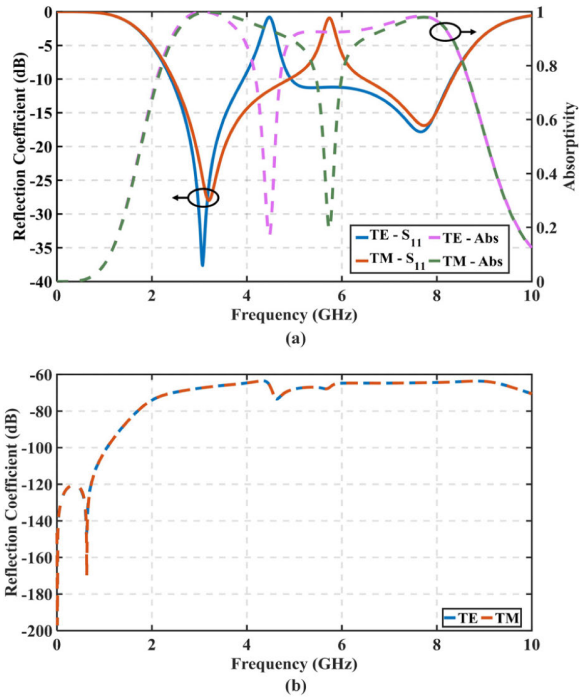

FIGURE 10. Simulated (a) co-polarized reflection coefficient and absorptivity and (b) cross-polarized reflection coefficient of the proposed FSA-R.

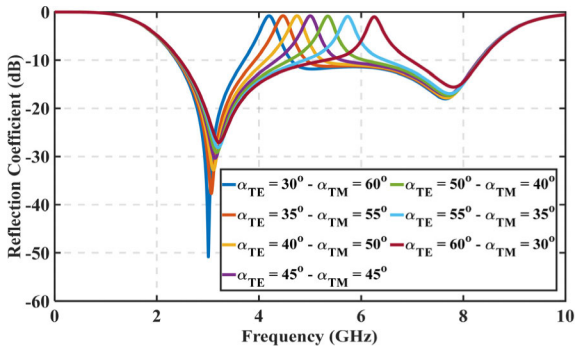

FIGURE 11. Variation in reflection coefficient of the proposed FSA-R for different values of α.

an intense surface current is observed at the TE polarization reflection frequency ($f_{TE} = 4.47$ GHz) and mainly along the y-direction. On the contrary, the surface current excited on the lossless FSS at a frequency of $f_{TM} = 5.74$ GHz is very low. In other words, the lossless FSS allows incoming waves to pass through, and the FSA-R works as an absorber at this frequency. Fig. 14 (c)-(d) illustrates the current distribution for TM polarized wave. A similar discussion as in the case of TE polarization can be made about the current distribution for the TM polarized wave.

C. SENSITIVITY TO OBLIQUE INCIDENCE

The performance of the proposed FSA-R under oblique incidence was investigated for both TE and TM polarizations, as shown in Fig. 15(a)-(b), respectively. The oblique incidence angle is varied from 0° to 30° in steps of 10°. Under

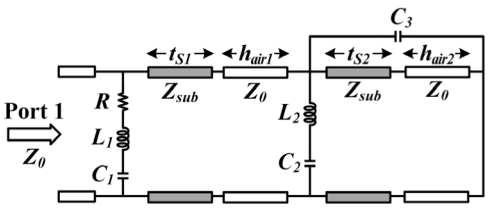

FIGURE 12. ECM of the proposed FSA-R.

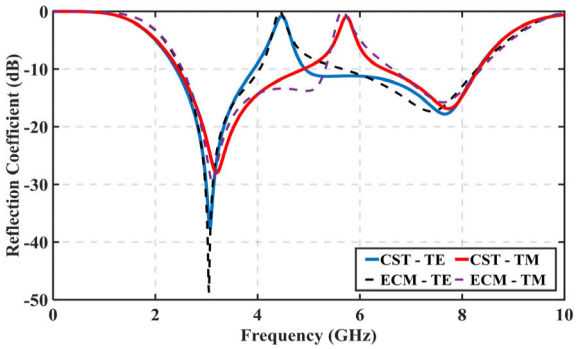

FIGURE 13. Simulated reflection coefficient of the proposed FSA-R by using CST and ECM.

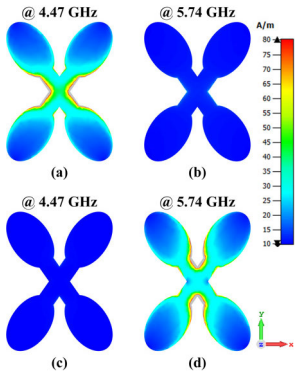

FIGURE 14. Current distribution for (a)-(b) TE and (c)-(d) TM polarized wave.

TE polarization, the reflection band is stable up to 30°; meanwhile, the lower absorption band is relatively stable, but the absorption bandwidth at higher frequencies narrows slightly with the increment of the incident angle. Under TM polarization, both the reflection and absorption bands are stable up to 20°.

D. RADAR CROSS SECTION

The bi-static RCS of the proposed FSA-R with dimensions of 300 mm × 300 mm (15 × 15 unit cells) and a PEC plate of the same size have been compared using the CST software to assess the competency of the proposed FSA-R for RCS reduction applications. The bi-static RCS for both TE and TM polarized normal incident waves in the E-plane are depicted in Fig. 16(a)-(c) in terms of reflection angle (Theta) at three distinct frequencies. At the absorption frequency of 3 GHz, the bi-static RCS of the FSA-R in all directions is reduced compared with that of the PEC plate for both polarizations. At 4.47 GHz frequency, almost all incident

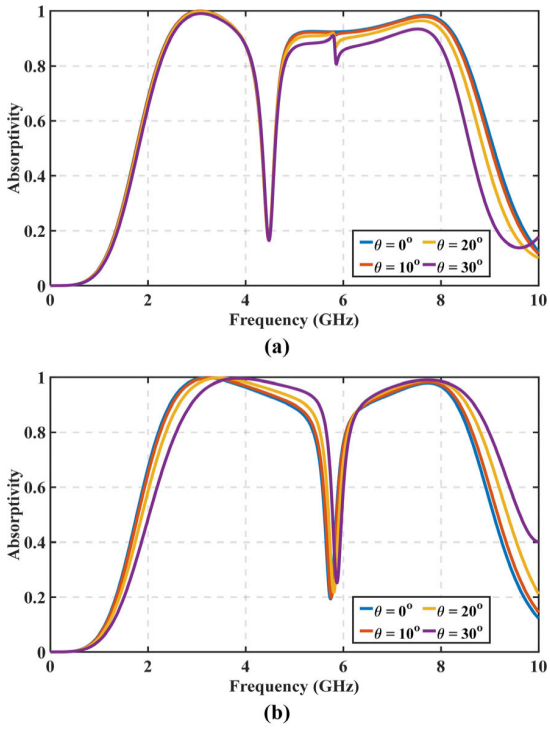

FIGURE 15. Simulated absorptivity of the proposed FSA-R under different incident angles for (a) TE and (b) TM polarizations.

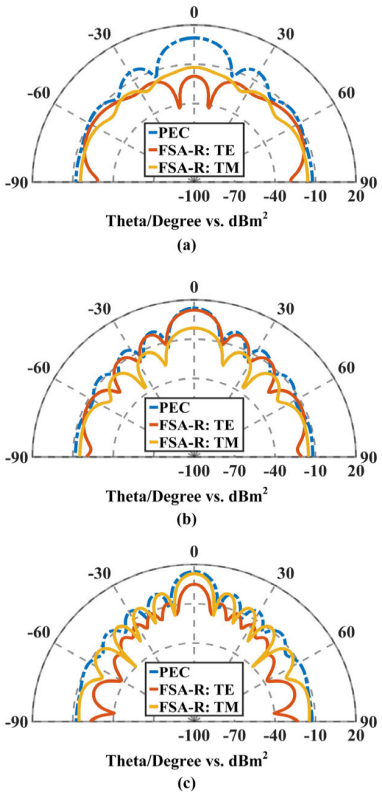

FIGURE 16. Bi-static RCS comparison of PEC and the proposed FSA-R at (a) $f_a = 3$ GHz, (b) $f_b = 4.47$ GHz and (c) $f_c = 5.74$ GHz.

waves are reflected in TE polarization, as the FSA-R behaves like a PEC plane. Conversely, for TM polarized waves, the

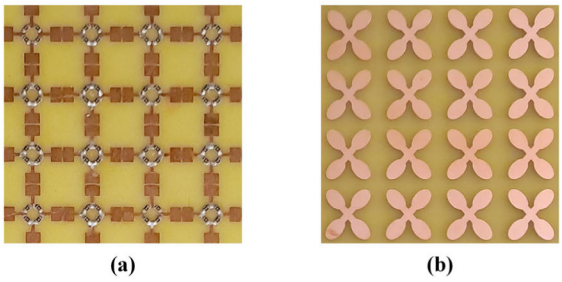

FIGURE 17. Photograph of fabricated prototype of the proposed FSA-R. Enlarged view of (a) lossy layer and (b) lossless layer.

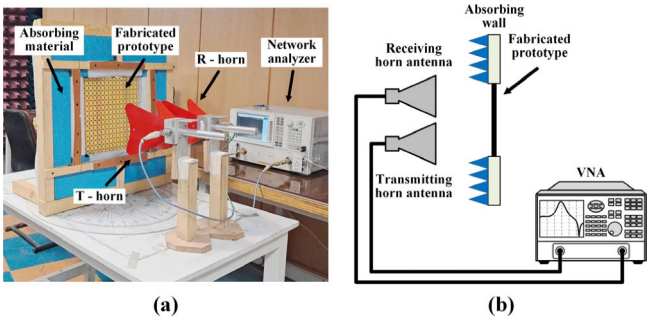

FIGURE 18. (a) Photography and (b) block diagram of the measurement setup.

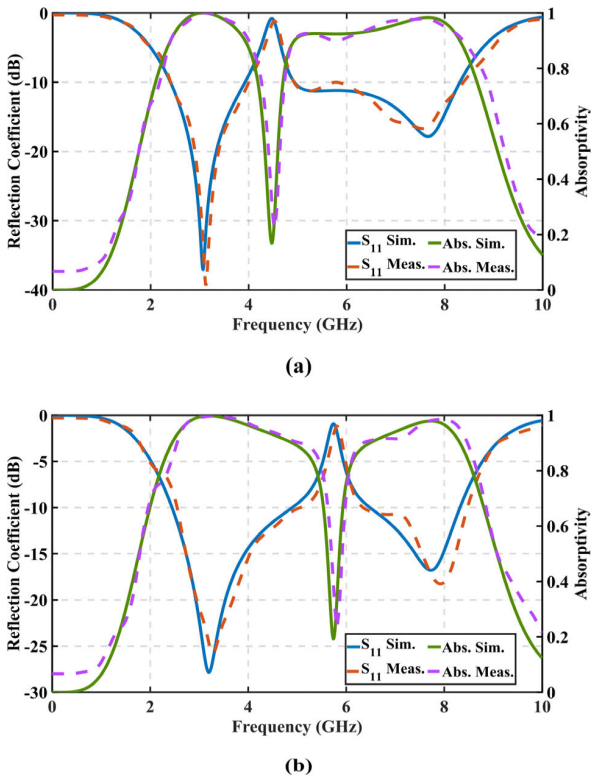

FIGURE 19. Simulated and measured reflection and absorptivity of the proposed FSA-R under normal incidence for (a) TE and (b) TM polarizations.

RCS is noticeably reduced in the entire space compared to that of PEC. A similar discussion can be made for RCS at 5.74 GHz.

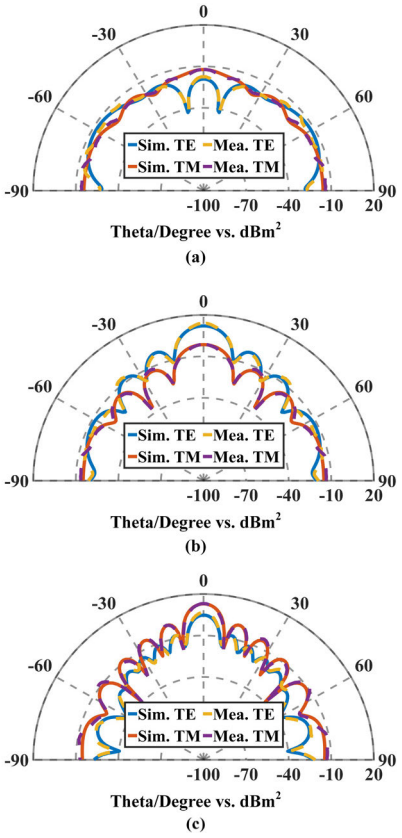

FIGURE 20. Simulated and measured bistatic RCS of the proposed FSA-R at (a) $f_a = 3$ GHz, (b) $f_b = 4.47$ GHz and (c) $f_c = 5.74$ GHz.

V. EXPERIMENTAL VERIFICATION

A 300×300 mm^2 prototype consisting of 15×15 unit cells has been fabricated to experimentally verify the proposed structure as illustrated in Fig. 17. The top and intermediate layers were printed on the FR4 dielectric substrates using the printed circuit board technique. Besides, a copper-cladded sheet was used as the ground plane. The substrate's relative permittivity and loss tangent are 4.4 and 0.02, respectively. Plastic screws and nuts are used to fix the required air gaps between layers. The lumped resistors of 200 Ω (0805 package) were soldered manually onto the lossy layer.

Fig. 18 shows the full view of the measurement setup. The free space technique is exploited to carry out the measurements [39]. The fabricated prototype is fixed within an absorbing foam frame to eliminate the scattering and diffraction of electromagnetic waves during measurement.

Two dual-ridged horn antennas (ETS-LINDGREN 3117) are used for transmitting and receiving the test electromagnetic wave. Both antennas are placed in front of the fabricated prototype. The reflection coefficients are measured by a vector network analyzer (Agilent E8363C). Enough far field distance is maintained between the antennas and the structure to comply with the plane wave conditions. In order to assess the angular stability of the structure, transmitting and receiving horn antennas are rotated manually to change the angle of the incident wave.

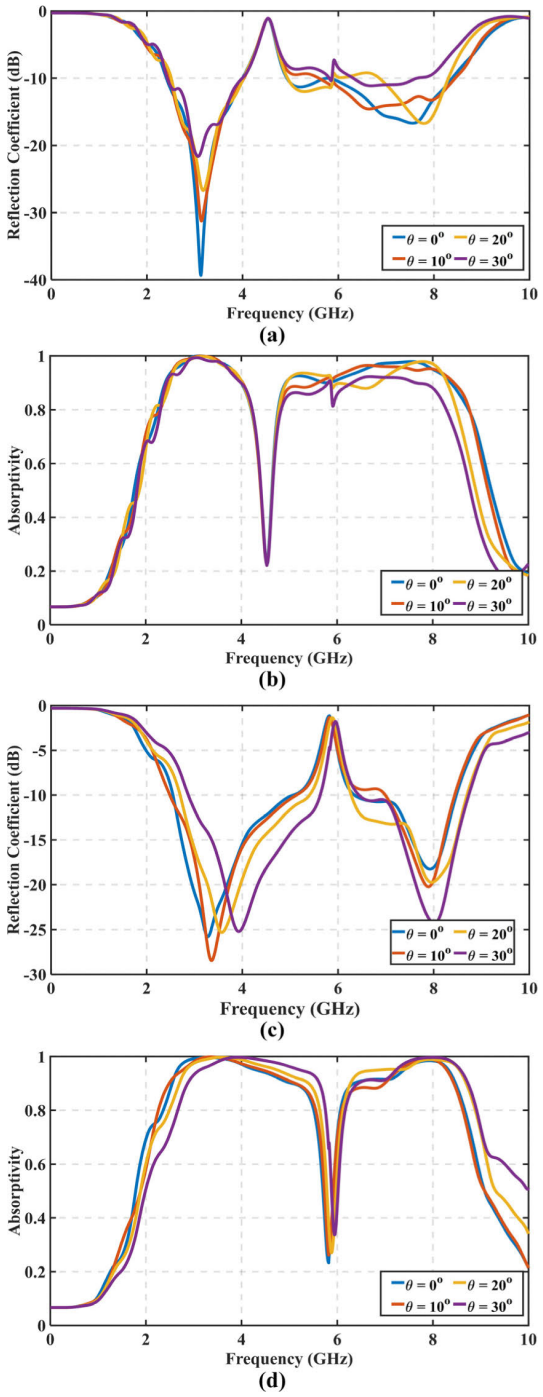

FIGURE 21. Measured reflection and absorptivity of the proposed FSA-R under oblique incidence for (a)-(b) TE and (c)-(d) TM polarizations.

Fig. 19 demonstrates the comparison of the measured and simulated performance of the FSA-R under normal incidence. As is clear, there is a good agreement between the results, proving the proposed structure's proper functionality. The slight discrepancy can be ascribed to the geometry tolerance, the parasitic effect of the lumped resistors, variation of the substrates' dielectric constant, misalignment of the device under test and horn antennas, measurement errors, etc.

TABLE 1. Performance comparisons between the proposed FSA-R and previously reported designs.

Refs.	Reflection notch / Loss	Cell Size (mm)	Thickness (mm)	Reflection band Attribute
[16]	7.54 GHz , -0.03 dB 13.25 GHz , -0.1 dB	16 ($2.04\lambda_L^2$) × 16 ($2.04\lambda_L$)	6.04 ($0.09\lambda_L$)	Polarization Insensitive
[20]	3.54 GHz , -0.12 dB	25 ($0.17\lambda_L$) × 25 ($0.17\lambda_L$)	13 ($0.089\lambda_L$)	Polarization Insensitive
[21]	wideband: 8.2-9.8 GHz , DNG[1]	16 ($0.26\lambda_L$) × 11.4 ($0.18\lambda_L$)	6.5 ($0.104\lambda_L$)	Single Polarized
[22]	10 GHz , -0.45 dB	10.2 ($0.18\lambda_L$) × 10.2 ($0.18\lambda_L$)	5.05 ($0.09\lambda_L$)	Polarization Insensitive
[23]	4.56 GHz , -1.63 dB	18 ($0.12\lambda_L$) × 18 ($0.12\lambda_L$)	17.81 ($0.09\lambda_L$)	Polarization Insensitive
This work	**TE:** 4.47 GHz , -0.8 dB **TM:** 5.74 GHz , -0.9 dB	20 ($0.16\lambda_L$) × 20 ($0.16\lambda_L$)	11.5 ($0.09\lambda_L$)	Anisotropic

[1]DNG = data not given, [2]λ_L = free-space wavelength at the lowest operating frequency.

Fig. 20 shows the comparative analysis of simulated and measured bi-static RCS for the proposed FSA-R at three distinct frequencies. The outlined procedure in [13] was utilized to assess the RCS experimentally. The transmitting horn antenna is kept stationary such that the incident wave falls perpendicularly onto the fabricated prototype. The receiving horn antenna is moved gradually in a circular path, and the reflection coefficient is measured using the network analyzer at each step. The results prove that a reasonable agreement exists between simulated and measured data. Also, the performance of the fabricated FSA-R under oblique incidences is investigated in Fig. 21.

A comparison is provided in Table 1 to verify the performance of the proposed FSA-R versus the recently reported designs in the literature. Since the experimental methods of each work differ from the others, it is not fair to compare them according to the measurement results. Compared with the reported FSA-Rs, only the proposed FSA-R yields an anisotropic reflection band.

VI. CONCLUSION

In this paper, a 2-D triple-layered AFSR with an anisotropic reflection band was proposed. A wideband absorber structure was constructed by placing a lossy FSS above a metal plane. A lossless FSS whose unit cell comprises two non-perpendicular dipole-shaped patches was added between two layers to produce an anisotropic reflection band. The frequency behavior of the proposed FSA-R was investigated using the equivalent circuit method. Extensive simulations were carried out to assess the performance of the presented structure. The proposed design exhibits the reflective notch frequencies of $f_{TE} = 4.47$ GHz and $f_{TM} = 5.74$ GHz under TE and TM polarizations, respectively. A 300 × 300 mm^2 prototype consisting of 15 ×15 unit cells has been fabricated to validate the performance of the FSA-R. Measured results were in good agreement with the simulated ones, verifying the validity of the design concept and procedure.

REFERENCES

[1] S. Guo, C. Hu, and H. Zhang, "Unidirectional ultrabroadband and wide-angle absorption in graphene-embedded photonic crystals with the cascading structure comprising the Octonacci sequence," *J. Opt. Soc. Amer. B, Opt. Phys.*, vol. 37, no. 9, p. 2678, Sep. 2020.

[2] Z. Guo, C. Gao, and H. Zhang, "Direction-dependent Janus metasurface supported by waveguide structure with spoof surface plasmon polariton modes," *Adv. Mater. Technol.*, vol. 8, no. 2, Nov. 2022, Art. no. 2200435.

[3] J. Qu, H. Pan, Y. Sun, and H. Zhang, "Multitasking device regulated by the gravity field: Broadband anapole-excited absorber and linear polarization converter," *Annalen der Physik*, vol. 534, no. 9, Jul. 2022, Art. no. 2200175.

[4] Y. Sun, D. Zhang, and H. Zhang, "Tailoring dual-band electromagnetically induced transparency with polarization conversions in a dielectric-metal hybrid metastructure," *Opt. Exp.*, vol. 30, no. 17, p. 30574, Aug. 2022.

[5] T. Guo, M. Guo, X. Jia, Q. Chen, and Y. Fu, "An absorptive frequency selective reflector with wide reflection band," *IEEE Access*, vol. 8, pp. 124217–124222, 2020.

[6] M. M. Zargar, A. Rajput, K. Saurav, and S. K. Koul, "Low RCS dual-polarized crossed dipole antenna co-designed with absorptive frequency-selective reflection structure," *IEEE Access*, vol. 10, pp. 118806–118814, 2022.

[7] M. Qu, T. Chang, G. Guo, and S. Li, "Design of graphene-based dual-polarized switchable rasorber/absorber at terahertz," *IEEE Access*, vol. 8, pp. 127220–127225, 2020.

[8] S. C. Bakshi, D. Mitra, and F. L. Teixeira, "Multifunctional frequency selective rasorber with dual mode and continuous tunability," *IEEE Trans. Antennas Propag.*, vol. 69, no. 9, pp. 5704–5715, Sep. 2021.

[9] M. Guo, T. Guo, Q. Cheng, Y. Zheng, and Y. Fu, "Frequency selective rasorber with anisotropic transmission band," *IEEE Antennas Wireless Propag. Lett.*, vol. 20, no. 2, pp. 155–159, Feb. 2021.

[10] Z. Wang, J. Fu, Q. Zeng, M. Song, and T. A. Denidni, "Wideband transmissive frequency-selective absorber," *IEEE Antennas Wireless Propag. Lett.*, vol. 18, no. 7, pp. 1443–1447, Jul. 2019.

[11] X. Kong, L. Kong, S. Jiang, X. Wang, Y. Zou, and L. Xing, "Low-profile and dual-polarization water-based frequency selective rasorber with ultrawideband absorption," *IEEE Antennas Wireless Propag. Lett.*, vol. 20, no. 12, pp. 2534–2538, Dec. 2021.

[12] A. Malekara, A. Khalilzadegan, C. Ghobadi, and J. Nourinia, "Wide-angle, dual-polarized frequency selective rasorber based on the electric field coupled resonator using characteristic mode analysis," *J. Appl. Phys.*, vol. 133, no. 16, Apr. 2023, Art. no. 164504.

[13] M. M. Zargar, A. Rajput, K. Saurav, and S. K. Koul, "Frequency-selective rasorber based on high-Q Minkowski fractal-shaped resonator for realizing a low radar cross-section radiating system," *IEEE Trans. Electromagn. Compat.*, vol. 64, no. 5, pp. 1574–1584, Oct. 2022.
[14] Y. Yu, G. Q. Luo, A. A. Omar, X. Liu, W. Yu, Z. C. Hao, and Z. Shen, "3D absorptive frequency-selective reflection and transmission structures with dual absorption bands," *IEEE Access*, vol. 6, pp. 72880–72888, 2018.
[15] A. A. Omar, H. Huang, and Z. Shen, "Absorptive frequency-selective reflection/transmission structures: A review and future perspectives," *IEEE Antennas Propag. Mag.*, vol. 62, no. 4, pp. 62–74, Aug. 2020.
[16] X. J. Hao, X. Q. Lin, X. M. Yang, Y. H. Su, Y. Yao, and Y. L. Yang, "Dual-polarized dual-band-notched frequency-selective absorber with high design freedom," *IEEE Antennas Wireless Propag. Lett.*, vol. 22, no. 1, pp. 59–63, Jan. 2023.
[17] Y. Han, Y. Chang, and W. Che, "Frequency-selective rasorbers: A view of frequency-selective rasorbers and their application in reducing the radar cross sections of antennas," *IEEE Microw. Mag.*, vol. 23, no. 2, pp. 86–98, Feb. 2022.
[18] B. Zhang, L. Li, C. Jin, Q. Lv, and R. Mittra, "Wideband low RCS antenna based on hybrid absorptive-diffusive frequency selective reflector," *IEEE Access*, vol. 9, pp. 77863–77872, 2021.
[19] A. Sharma, S. Ghosh, and K. V. Srivastava, "A polarization-insensitive band-notched absorber for radar cross section reduction," *IEEE Antennas Wireless Propag. Lett.*, vol. 20, no. 2, pp. 259–263, Feb. 2021.
[20] Y. Han, L. Zhu, Y. Chang, and B. Li, "Dual-polarized bandpass and band-notched frequency-selective absorbers under multimode resonance," *IEEE Trans. Antennas Propag.*, vol. 66, no. 12, pp. 7449–7454, Dec. 2018.
[21] P. Mei, X. Q. Lin, J. W. Yu, and P. C. Zhang, "A band-notched absorber designed with high notch-band-edge selectivity," *IEEE Trans. Antennas Propag.*, vol. 65, no. 7, pp. 3560–3567, Jul. 2017.
[22] Y. Ding, M. Li, J. Su, Q. Guo, H. Yin, Z. Li, and J. Song, "Ultrawideband frequency-selective absorber designed with an adjustable and highly selective notch," *IEEE Trans. Antennas Propag.*, vol. 69, no. 3, pp. 1493–1504, Mar. 2021.
[23] Y. Fan, D. Li, H. Ma, J. Xing, Y. Gu, L. K. Ang, and E.-P. Li, "Ultrawideband dual-polarized frequency-selective absorber with tunable reflective notch," *IEEE Trans. Antennas Propag.*, vol. 71, no. 3, pp. 2855–2860, Mar. 2023.
[24] H. Huang, Z. Shen, and A. A. Omar, "3-D absorptive frequency selective reflector for antenna radar cross section reduction," *IEEE Trans. Antennas Propag.*, vol. 65, no. 11, pp. 5908–5917, Nov. 2017.
[25] X. Xiu, W. Che, W. Yang, Y. Han, and Q. Xue, "Double-polarized dual-passband absorptive frequency-selective transmission structure," *IEEE Trans. Electromagn. Compat.*, vol. 62, no. 5, pp. 1951–1960, Oct. 2020.
[26] X. Zhang, H. Ma, J. Wang, S. Zhou, and H. Liu, "Game theory design for deceptive jamming suppression in polarization MIMO radar," *IEEE Access*, vol. 7, pp. 114191–114202, 2019.
[27] J. Yang, J. Li, S. Zhou, D. Li, and G. Yang, "A polarization and frequency reconfigurable microstrip antenna for vehicular communication system application," *IEEE Trans. Veh. Technol.*, vol. 72, no. 1, pp. 623–631, Jan. 2023.
[28] S. C. Bakshi, D. Mitra, and L. Minz, "A compact design of multiband terahertz metamaterial absorber with frequency and polarization tunability," *Plasmonics*, vol. 13, no. 6, pp. 1843–1852, Dec. 2018.
[29] R. Bajracharya, R. Shrestha, S. A. Hassan, H. Jung, and H. Shin, "5G and beyond private military communication: Trend, requirements, challenges and enablers," *IEEE Access*, vol. 11, pp. 83996–84012, 2023.
[30] M. Li, S. Xiao, Y.-Y. Bai, and B.-Z. Wang, "An ultrathin and broadband radar absorber using resistive FSS," *IEEE Antennas Wireless Propag. Lett.*, vol. 11, pp. 748–751, 2012.
[31] F. Costa, A. Monorchio, and G. Manara, "Analysis and design of ultra thin electromagnetic absorbers comprising resistively loaded high impedance surfaces," *IEEE Trans. Antennas Propag.*, vol. 58, no. 5, pp. 1551–1558, May 2010.
[32] D. M. Pozar, *Microwave Engineering*, 2nd ed. Toronto, ONT, Canada: Wiley, 1998.
[33] Q. Zhou, M. Guo, H. Moghadas, Z. Wu, P. Liu, and M. Daneshmand, "A frequency selective rasorber with three transmission bands and three absorption bands," *IEEE Access*, vol. 7, pp. 160973–160981, 2019.
[34] Q. Chen, D. Sang, M. Guo, and Y. Fu, "Frequency-selective rasorber with interabsorption band transparent window and interdigital resonator," *IEEE Trans. Antennas Propag.*, vol. 66, no. 8, pp. 4105–4114, Aug. 2018.
[35] S. Mahmud, M. Karim, S. S. Islam, M. M. K. Shuvo, T. Akter, A. F. Almutairi, and M. T. Islam, "A multi-band near perfect polarization and angular insensitive metamaterial absorber with a simple octagonal resonator for visible wavelength," *IEEE Access*, vol. 9, pp. 117746–117760, 2021.
[36] O. Luukkonen, C. Simovski, G. Granet, G. Goussetis, D. Lioubtchenko, A. V. Raisanen, and S. A. Tretyakov, "Simple and accurate analytical model of planar grids and high-impedance surfaces comprising metal strips or patches," *IEEE Trans. Antennas Propag.*, vol. 56, no. 6, pp. 1624–1632, Jun. 2008.
[37] S. Sheikh, "Miniaturized-element frequency-selective surfaces based on the transparent element to a specific polarization," *IEEE Antennas Wireless Propag. Lett.*, vol. 15, pp. 1661–1664, 2016.
[38] X.-C. Wei, *Modeling and Design of Electromagnetic Compatibility for High-Speed Printed Circuit Boards and Packaging*. Boca Raton, FL, USA: CRC Press, 2017.
[39] D. S. Wang, P. Zhao, and C. H. Chan, "Design and analysis of a high selectivity frequency-selective surface at 60 GHz," *IEEE Trans. Microw. Theory Techn.*, vol. 64, no. 6, pp. 1694–1703, Jun. 2016.

ASAL MALEKARA received the B.S. and M.Sc. degrees in electrical engineering from Urmia University, Urmia, in 2010 and 2013, respectively, where she is currently pursuing the Ph.D. degree in communication engineering with the Department of Electrical Engineering. Her current research interests include the design of frequency selective surfaces and frequency selective absorbers.

CHANGIZ GHOBADI received the B.Sc. degree in electrical engineering and the M.Sc. degree in electrical engineering telecommunication from the Isfahan University of Technology, Isfahan, Iran, and the Ph.D. degree in electrical telecommunication from the University of Bath, Bath, U.K., in 1998. He is currently a Professor with the Department of Electrical Engineering, Urmia University, Urmia, Iran. He has supervised and administered more than 130 M.Sc. and 32 Ph.D. students and their thesis. He has authored and coauthored more than 360 scientific publications, including accredited journals and conferences. His articles have been cited more than 5750 times. His current research interests include antenna design, radar, and adaptive filters. He has been included in the top 1 % of the world's scientists and academics according to Thomson Reuters' list, in 2017, 2020, and 2022.

JAVAD NOURINIA (Senior Member, IEEE) received the B.Sc. degree in electrical and electronic engineering from Shiraz University, the M.Sc. degree in electrical and telecommunication engineering from the Iran University of Science and Technology, and the Ph.D. degree in electrical and telecommunication from the University of Science and Technology, Tehran, Iran, in 2000. He was the Head of the Faculty of Engineering, from 2013 to 2017, and a Distinguished Professor with Urmia University. His current research interests include small antennas, filters, MIMO antennas, periodic structures, optimization, and measurement. He has been included in the top 1 % of the world's scientists and academics according to Thomson Reuters' list, since 2016.